RSC Advances

PAPER

View Article Online
View Journal | View Issue

Cite this: *RSC Adv.*, 2016, **6**, 9013

Determination of concentration-dependent diffusion coefficient of seven solvents in polystyrene systems using FTIR-ATR technique: experimental and mathematical studies

Mohammad Karimi,*[a] Akbar Asadi Tashvigh,[b] Fateme Asadi[a] and Farzin Zokaee Ashtiani[b]

In the present study a new mathematical model's outcome based on experimental data is considered to determine the diffusion coefficients in polystyrene/solvent systems as a function of solvent concentration. We used a calibrated Fourier transform infrared attenuated total reflectance (FTIR-ATR) instrument to collect the spectra from a thin layer of polymer solution covered optically dense ZnSe crystal. The collected spectra were transferred to the components' concentration, using principal component regression analysis, representing the compositional change of the polymer solution during the time. Two approaches were employed to obtain the diffusion coefficients of seven solvents in polystyrene solutions: first, we considered whole range of polymer concentration to obtain the diffusion coefficient by fitting the diffusion model on experimental data. In the second approach only early stage of evaporation process was figured, considering vitrification phenomenon in the upper layers of polymer solution film. For all solvents, higher values of diffusion coefficients obtained using second approach, showing a satisfying agreement with the literature. As a concluding remark, vitrification is an important event taken place during mass transfer processes in which it should be considered to find a reliable value for diffusion coefficient.

Received 27th November 2015
Accepted 13th January 2016

DOI: 10.1039/c5ra25244j

www.rsc.org/advances

1. Introduction

Diffusion of solvent in polymeric systems is of major importance in a number of applications, including fiber formation,[1,2] membrane manufacturing,[3–6] and foaming processes.[7] In these processes, solvent molecules evaporate or are released from cast polymer solution into the atmosphere or a liquid bath. The process will continue with an arrangement of polymer chains in a special structure which is affected by solvent diffusion mechanism.[8–10] On the other hand, during the mass transfer, diffusion of solvent affects polymer concentration as well as mobility of polymer molecules. The latter case is controlled by glass transition temperature of the mixture, that is $T_{g,mix}$. For the duration of solvent outflow, the $T_{g,mix}$ rises to overtake processing temperature whether a polymer with T_g higher than processing temperature is selected; indeed at $T = T_{g,mix}$ the polymer chains become frozen. This is while, the solid state and solution state differ on diffusion behavior.[1] The solvent diffusion through internal layers of sample depends on the boundary layer state. Solidification of this outermost layer affects the diffusion process of internal layers. Little is known about the solvent diffusion coefficient with relation to internal layers when the boundary layer solidifies. Obtaining such information can help to understand the morphological evolution of materials.

Many attempts have been made to measure and predict the diffusion coefficient of solvent in polymer solutions.[11–20] A general method of measuring is determining the solvent evaporation rate. In particular, the gravimetric measurement of the solvent evaporated from appropriate cast polymer–solvent films are carried out through the experiments; such measurements provide no information about the concentration gradient of internal layers. In contrast analyzing the bottom layer of the cast polymer–solvent mixture using Fourier transmission infrared (FTIR) has been recently used as a robust experimental technique to determine the diffusion coefficient.[15,21–27] Fieldson and Barbari[22] have successfully used FTIR-ATR spectroscopy, as a novel approach for measuring the diffusion coefficient of liquid water in polyacrylonitrile systems. Fu and Lim[23] used FTIR-ATR technique to investigate the multiple-component diffusion properties of 2-octanone, hexyl acetate, octanal, limonene and linalool in a linear low density polyethylene film. The investigation results were successfully validated using data

[a]*Department of Textile Engineering, Amirkabir University of Technology, No. 15914, Hafez Ave., 15914 Tehran, Iran. E-mail: mkarimi@aut.ac.ir; Fax: +98-21-66400245; Tel: +98-21-64542658*

[b]*Department of Chemical Engineering, Amirkabir University of Technology, No. 15914, Hafez Ave., 15914 Tehran, Iran*

from the literature. Hanh *et al.*,[24] have successfully showed that FTIR-ATR technique is applicable for determining the diffusion coefficient of drugs in semisolids. Hong *et al.*[25] have measured the diffusion coefficients of toluene/methyl ethyl ketone (MEK) mixtures in polyisobutylene at 50 °C using vapor sorption FTIR-ATR spectroscopy. They also showed that diffusion coefficient of penetrant is strongly affected by concentration gradient. Finally Elabd *et al.*[28] presented a review about the application of FTIR-ATR spectroscopy in measuring of diffusion coefficient in polymers.

In this work we are motivated to use FTIR technique for measuring the concentration variation of solvent through internal layers of cast polymer–solvent films during solvent evaporation process. The bottom layer of cast polymer–solvent mixture is probed by capturing spectra at a rate of one per 0.2 second to quantify the solvent concentration in this layer. These data was then used to obtain diffusion coefficient of solvent applying mathematical methods.

2. Experimental

2.1. Material

Commercial grade of polystyrene (PS) (Solarene G144) with melt flow index of 8.5 (200 °C, 5 kg) was purchased from Dongbu Hannong Chemical Co (South Korea). The solvents: tetrahydrofuran (THF), acetone (AC), chloroform, dichloromethane (DCM), toluene, benzene, 1,4-dioxane and tetrachloroethylene (TCE) were obtained from Merck, Germany and used as received.

2.2. FTIR-ATR technique

According to the principle of ATR technique,[29] when a beam of infrared light propagates through a dense medium (an ATR crystal) in such a way that it reflects at least once off the internal surface in contact with a rarer medium (a polymer solution), attenuated total internal reflection (ATR) occurs. This reflection forms an evanescent wave which extends into the sample. The schematic of ATR crystal is depicted in Fig. 1.

The polymer solutions (15 wt%) were precisely prepared by dissolving the specific quantity of polymer in appropriate solvent at room temperature, continued with stirring until a clear polymer solution was obtained. Afterwards, it was cast directly on the surface of the flat crystal (ZnSe, refractive index 2.4 and incident angle 45°) equipped with a bottomless liquid cell. The depth of polymer solution which defines the film thickness was controlled by a blade, together with keeping the interfacial area of polymer solution under control to firmly set a 1.35 cm^2 of area by a frame, made of nonabsorbent material. Before collecting the spectra, FTIR-ATR was calibrated by spectrum of background under steady flow of N_2 purge; this was performed under 40 scans and 4 cm^{-1} spectral resolution; the wavenumber range was 650–4000 cm^{-1}. The spectra for all samples were recorded at 0.2 second intervals after casting the solution on the ATR crystal. FTIR-ATR spectrum was measured using a Nexus 670 (Nicolet) spectrometer in kinetic mode.

The penetration depth of the IR beam in polymer solution sample can be calculated by eqn (1).

$$d_p = \frac{\lambda}{2\pi\sqrt{n_1^2 \sin^2\theta - n_2^2}} \quad (1)$$

where penetration depth of evanescent wave is shown by d_p, λ is the wavelength of the infrared radiation, n_1 and n_2 are the refractive indices of flat crystals and polymer solutions respectively and θ is the angle of incidence beam.[29,30]

Fig. 2 shows the spectra collected from PS/THF solution under evaporation process. Evaporating the THF from top surface of solution causes to form a concentration gradient under diffusion control. After a period of time, a change in concentration is detected at the bottom-surface of solution which is a typical layer of ATR analyzing. As seen in Fig. 2, a gradually decrement of intensity is observed for the characteristic peak of THF in region between 2800 cm^{-1} and 2900 cm^{-1}, indicating that the THF molecules at the bottom layer of polymer solution, in contact with ATR prism, decrease because of evaporation. In contrast, an increase of intensity is observed for characteristic peak of PS in region between 2900 cm^{-1} and 2950 cm^{-1}, in which it means that PS concentration increases with time.

To determine the solvent concentration in the cast PS solution, the IR spectra were quantified using TQ ANALYST software by means of principal component regression (PCR) technique.[31] Calibration of the system was accomplished by capturing spectrum from pure components and also binary mixtures of

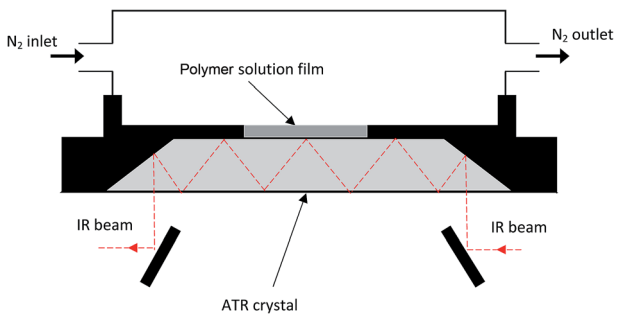

Fig. 1 Description of the main concepts of ATR-FTIR spectroscopy applied to the study of diffusion in polymer solution.

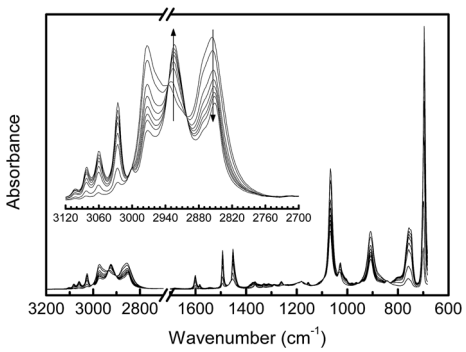

Fig. 2 ATR-FTIR spectrum of polystyrene/THF solution during evaporation of THF as function of time in the region of 600–4000 cm^{-1}.

each solvents and polystyrene. PCR technique provides the possibility of decoupling and calibrating the component peaks or regions that overlap. Basic knowledge of using FTIR-ATR technique and quantifying concentration *via* analyzing the specified spectra have been presented elsewhere[11] that realizes this paper. This technique, based on measuring the FTIR-ATR spectrum and calibrating the system, can be most possibly employed to determine the composition of polymer solution at the layer close to ATR prism dynamically, as the intensity of the characteristic peak changes.

3. Mathematical modeling

In this work, laboratory experiments were combined with mathematical modeling, in order to evaluate the accuracy of diffusion coefficient prediction. In particular, the laboratory experiments consist of detecting solvent concentration at the bottom layer of polymer solution film (PSF) during the time using ATR-FTIR technique stated above. The experimentally amount of evaporated solvent was compared with model predictions, in order to estimate the unknown parameters of the diffusion coefficient model.

The PSF which is depicted in Fig. 3, was considered as a rectangular layer with dimensions of 0.540 × 7 × 20 mm as height, width and length, respectively. According to the geometrical dimensions, the ratio of height (H) with respect to width (W) and length (L) of the PSF is far less than unity, *i.e.* $H/W \cong 0.07$ and $H/L \cong 0.027$. Hence the effect of mass diffusion in directions of x and z was neglected,[32] and the model was intended to be one-dimensional for mathematical calculations.

3.1. Governing equations

The unsteady-state mass transport equation is

$$\frac{\partial C}{\partial t} = \frac{\partial}{\partial y}\left(D(C)\frac{\partial C}{\partial y}\right) \tag{2}$$

where, C is the concentration of solvent, and $D(C)$ is diffusion coefficient of solvent, which may be a function of concentration.

Initial and boundary conditions for the diffusion equation are as follow:

$$C(y,0) = C_0 \text{ at } t = 0 \tag{3}$$

$$C(0,t) = C_{\text{FTIR}} \text{ for } y = 0 \tag{4}$$

$$-D(C)\frac{\partial C(H,t)}{\partial y} = k(C_e(t) - C_\infty) \tag{5}$$

Eqn (3) provides the initial concentration for solvent. Eqn (4) specifies the solvent concentration in the layer facing the IR prism. C_{FTIR} is concentration data extracted from FTIR spectra. Eqn (5) is mass transfer balance at the top layer of PSF, where the solvent enters to the ambiance *via* convection mechanism. k is the mass transfer coefficient between PSF and ambient air, C_∞ indicates concentration of solvent vapor in ambient air, and $C_e(t)$ represents the concentration of solvent vapor in the air just adjacent to the surface of PSF, that is in equilibrium with $C(H,t)$. These concentrations are shown schematically in Fig. 4. In order to estimate k, an empirical relation was used as below:[33]

$$\text{Nu} = \frac{kL}{D_a} = 0.646\text{Re}^{0.5}\text{Sc}^{1/3} \tag{6}$$

where, Nu, Re and Sc are dimensionless number of Nusselt, Reynolds and Schmidt of ambient air, and D_a, is diffusion coefficient of solvent vapor in the air.

As shown in Fig. 4, $C_e(t)$ and $C(H,t)$, are in equilibrium, so, the activity of solvent that corresponds to $C_e(t)$ and $C(H,t)$ must be equal. The Flory–Huggins theory was employed to describe activity of solvent in PSF,[34] the procedure for calculation of $C_e(t)$ is described as below:

✓ The activity of solvent that corresponds to $C(H,t)$ was calculated as:

$$\ln(a(H,t)) = \ln(\varphi(H,t)) + \left(1 - \frac{v_s}{v_p}\right)(1 - \varphi(H,t)) + (1 - \varphi(H,t))^2\chi \tag{7}$$

where, a and φ are activity and volume fraction of solvent in PSF, v_p and v_s are the molar volume of polymer and solvent, respectively, and χ is the Flory–Huggins interaction parameter between polymer and solvent.

✓ The activities of $a(H,t)$ and $a_e(t)$, must be equal

$$a_e(t) = a(H,t) \tag{8}$$

where, $a_e(t)$ corresponds to activity of $C_e(t)$.

✓ As the concentration of solvent in ambient air fairly remains low during the test, ambient air was assumed to be ideal solution and activity of solvent was considered to be equal to its concentration; it means:

$$\varphi_e(t) = a_e(t) \tag{9}$$

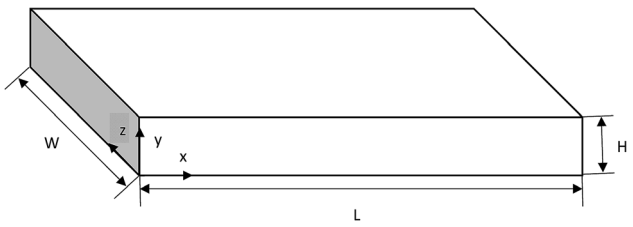

Fig. 3 Dimensions considered for polymer solution film in mathematical modelling.

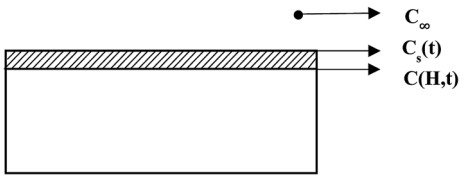

Fig. 4 Concentration boundary conditions around polymer solution film.

where, $\varphi_e(t)$ corresponds to volume fraction of $C_e(t)$.

✓ For conversion of $\varphi_e(t)$ to $C_e(t)$ the below equation was used

$$C_e(t) = \varphi_e(t)\rho_s \quad (10)$$

where, ρ_s is density of solvent vapor.

3.2. Diffusion coefficient model

To indicate the concentration dependency of diffusion coefficient of solvent in polymer, two linear and exponential models were introduced which are common diffusion models in literature[35–41] as below.

$$D(C) = D_0\, e^{\alpha C} \quad (11)$$

$$D(C) = D_0(1 + \alpha C) \quad (12)$$

where, D_0 and α are constant parameters.

3.3. Solution method

Eqn (2) was solved making an initial guess about D_0 and α in diffusion models (eqn (11) and (12)), in addition the solvent evaporation rate was calculated as below

$$J_s^{prd} = D(C)\frac{\partial C(H,t)}{\partial y} \quad (13)$$

where, J_s^{prd} is flux of solvent evaporation. So, the total amount of solvent, that vaporates would be (m_s^{prd})

$$m_s^{prd} = LW\int_0^{t_f} J_s^{prd}\mathrm{d}t \quad (14)$$

where t_f is the time that polymer solution solidifies.

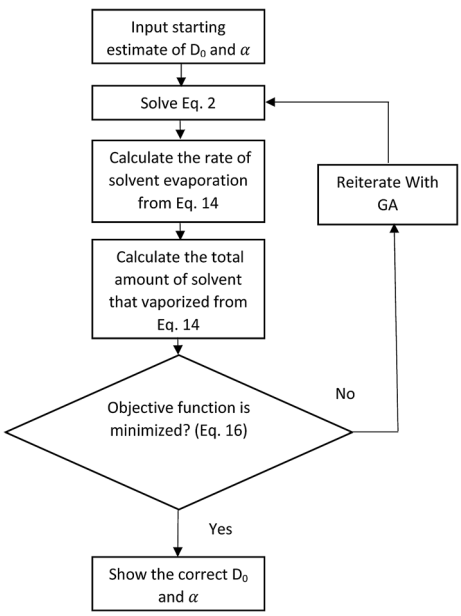

Fig. 5 Iterative procedure of mathematical solution to estimate diffusion coefficient of solvent in polystyrene.

To determine the diffusion coefficient's unknown parameters, the objective function was defined as

$$OF = |m_s^{prd} - m_s^{exp}| \quad (15)$$

where, m_s^{exp} is the amount of solvent evaporated, obtained experimentally. This objective function needs to be minimized by changing the D_0 and α. The genetic algorithm toolbox of Matlab software,[42,43] was supporting to minimize eqn (15). The procedure of solution is depicted in Fig. 5.

4. Results and discussion

Fig. 6 shows a series of spectra collected as a function of time during evaporation of THF from polystyrene (PS) solution. As the solvent evaporated, the intensity of characteristic peak of THF clearly decreases during the process (Fig. 6a), meaning that the solvent concentration decreases at the bottom layer of polymer solution film in contact with ATR prism. On the contrary, the peak specified at 1492 cm^{-1} grew in over 10 min since the beginning of the experiment and is assigned to the PS (Fig. 6b).

Using principal component regression (PCR) analysis, the concentration of THF was calculated, point to point during the evaporation process based on collected FTIR-ATR spectrum; the results are shown in Fig. 7. Data was collected under nitrogen atmosphere with flow rate of 100 ml min^{-1} at 25 °C

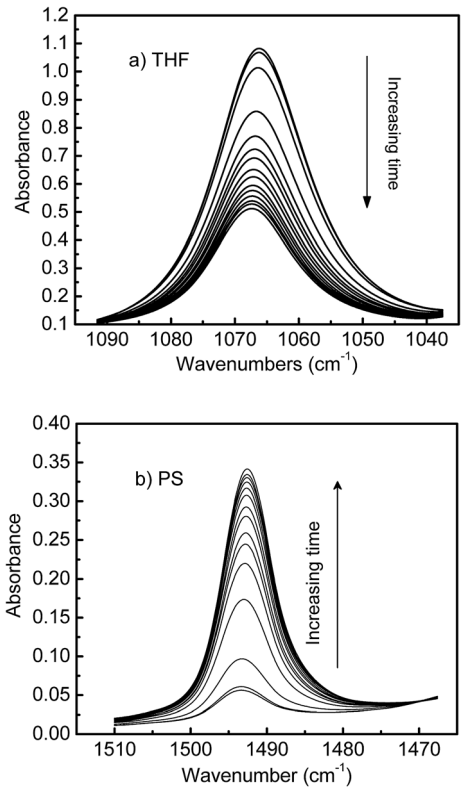

Fig. 6 Spectra of release of THF from PS solution; inset shows decrease of characteristic band of THF (a) as a function of time as well as the increase of characteristic band of PS (b) with time.

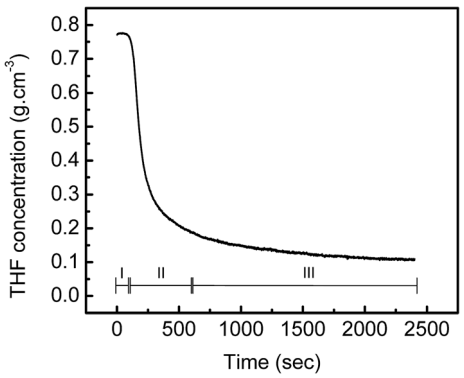

Fig. 7 THF concentration in PSF at interface of polymer solution and ATR prism obtained from calibrated instrument with use of principle component regression.

and thickness of 740 μm. Three regimes are recognized in Fig. 7. The first regime is related to initial delay time in propagating diffusion front; it moves from surface to bottom of polymer solution because of surface solvent evaporation. As solvent molecules are evaporating, the solvent concentration in bottom layer of PSF is reduced due to concentration gradient distributed throughout the thickness. This is the second regime that the weight loss of solvent starts and continues until the release of solvent becomes slow significantly; this is the beginning of third regime. This slowing of mass transfer rate is due to morphological state of polymer by which the vitrification phenomena on top layer of solution can happen. Vitrification is the transformation of solution into a glass if the glass transition of mixture overtakes the processing temperature.

To consider the physico-chemical nature of solvent on diffusion process, seven other solvents were selected for investigating in similar way as THF. Fig. 8 is representative of normalized solvents concentration during evaporation process in polystyrene solutions. As seen, the same trend and three regimes of evaporating process are observed for all solvents, but different types of kinetics are taken place.

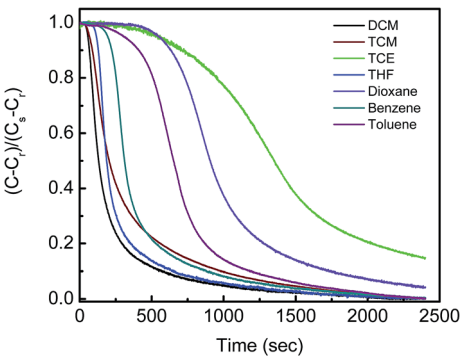

Fig. 8 Representative of normalized weight fraction of different solvents during solvent evaporation in polystyrene solutions.

4.1. Determination of diffusion coefficient model parameters

Preliminary works were done to figure out the degree of fitting between experimental data and diffusion models presented in eqn (11) and (12). Results showed that linear diffusion model (eqn (12)) is more capable to describe the mass transfer pattern in polymer solutions, and exhibits less error than exponential model (eqn (11)). The model's predicted outcomes for evaporated solvent were plotted *versus* its experimental values correspondingly in Fig. 9. As seen for all solvents, a good agreement was observed between linear model and experimental data. Parameters of diffusion coefficient models were obtained for all intended polymer/solvent mixtures and listed in Table 1. Spite of good agreement, the obtained diffusion coefficients are a bit lower than those reported in the literatures.[12–14,18,19] Structural variations during the process may be the key reasons of this discrepancy. Indeed, the rate of solvent evaporation is not constant during the drying process. It depends not only on concentration variation but also molecular structure of the media. When solvent molecules escape from the top layer of PSF, a transition from rubbery to glassy state may take place in polymer chains. Therefore, it can be expected that dynamics of solvent transport in the mixture follows by different behavior.

4.2. Effects of operating condition on applicability of the model

The diffusion model which earlier employed to evaluate the diffusion coefficient of THF in PS solution was assessed for various operating conditions. The experimental and predicted results for three various initial PSF thicknesses are depicted in Fig. 10. As shown, for PSF thickness lower than 740 μm, model tends to underestimate while it predicts an overestimated value for higher thicknesses than that. Two reasons are probably involved. The first is vitrification of top layer through which the glass transition of polymer/solvent mixture overtakes the processing temperature. At this situation, we expect the mass transfer rate to change. The second reason can be due to the essential assumption behind the calculation. Indeed, we considered the diffusion process as a one-dimensional model

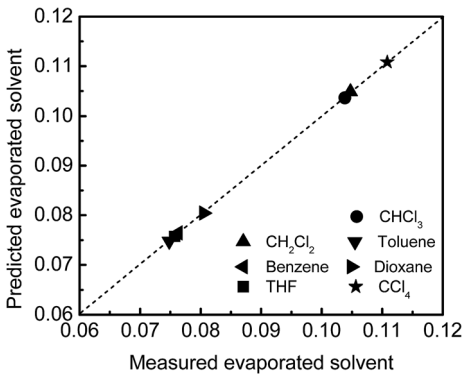

Fig. 9 Measured *versus* predicted evaporated solvent from PSF for initial thickness of 740 μm, nitrogen flowrate of 100 ml min^{-1} and temperature of 25 °C.

Table 1 Parameters of diffusion coefficient for various solvents

	Linear model			Exponential model		
Solvent	D_0 (m^2 s^{-1})	α	Percent of error	D_0 (m^2 s^{-1})	α	Percent of error
THF	4.91×10^{-10}	0.9321	0.00	7.18×10^{-10}	0.8928	27.63
$CHCl_3$	1.62×10^{-10}	1.6139	0.18	3.39×10^{-10}	0.7462	6.43
CH_2Cl_2	5.03×10^{-10}	0.9291	0.11	9.80×10^{-10}	0.6799	6.84
Toluene	2.86×10^{-10}	1.5344	0.06	2.20×10^{-10}	0.547	1.85
Benzene	6.50×10^{-10}	0.2512	0.16	2.41×10^{-10}	1.3909	13.75
Dioxane	1.71×10^{-10}	0.5624	0.10	6.06×10^{-11}	0.9912	26.97
C_2Cl_4	7.90×10^{-11}	0.1699	0.00	6.15×10^{-11}	0.9116	1.88

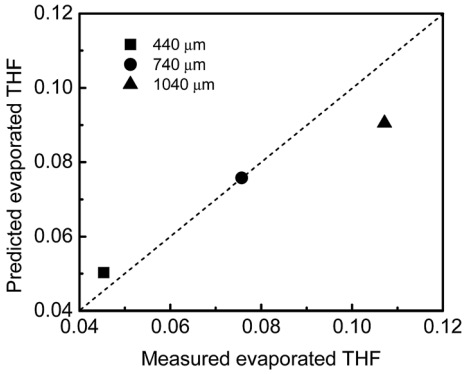

Fig. 10 Measured *versus* predicted evaporated THF from PSF for various thicknesses under nitrogen flowrate of 100 ml min^{-1} and temperature of 25 °C.

and also neglected the solvent evaporation from PSF side walls. In lower thicknesses, evaporated solvent from side walls was lower than that of 740 μm, therefore predicted evaporated solvent was more than that experimentally obtained. For higher thicknesses, evaporated solvent from side walls was more than that of 740 μm, therefore predicted value was lower than that experimentally measured.

Nitrogen flow rate purged the atmosphere of PSF was another operating condition for investigation. The experiment was carried out under two various nitrogen flow rates of 50 and 150 ml min^{-1}. The model predictions and experimental data of evaporated THF were plotted in Fig. 11 for comparison. It becomes clear from the picture that the difference between model outcomes and experiment data is not so significant. Indeed, the flow rate of nitrogen only changes the mass transfer coefficient (eqn (5)) but it does not affects the diffusion coefficient of solvent in the mixture; therefore, the mass transfer is only mechanism which dominates the evaporation process.

The last investigated parameter was the nitrogen gas flow temperature. The prediction and experimental values of evaporated solvent under various temperature are depicted in Fig. 12 to compare. As shown in Fig. 12, the model over predicts for all gas temperatures. As a reason for this observation, it is concluded that the gas temperature only changes the mass transfer coefficient and has no impact on diffusion coefficient of components. On the other hand, the change in gas temperature may just vary the temperature of upper layers of PSF in which we ignored its probable effect on reliability of predicted diffusion coefficient (eqn (12)).

4.3. Diffusion coefficient at the early stage

As stated earlier, the values of diffusion coefficients for all seven solvents in polystyrene solutions, presented in Table 1 are obtained by means of fitting technique. Indeed the diffusion model was fitted on experimental data in the whole range of concentration. According to the basic knowledge of polymer physics, the thermodynamic situation of polymers in solution state is related to its concentration. The motion of polymer chains is going to be slower when the solvent molecules evaporate more and more. At last, all polymer chains are frozen in spite of probably presence of solvent in the system, meaning that glass transition of mixture overtakes the process temperature; this is called vitrification. Consequently, as expected the diffusion mechanism changes to a new form when the mixture is at its glassy state. Table 2 summarizes the solvent concentrations of mixtures at their vitrification point. These values were calculated based on eqn (16).[32]

$$\frac{1}{T_{g,m}} = \frac{w}{T_{g,p}} + \frac{1-w}{T_{g,s}} \quad (16)$$

where, w is the polymer weight fraction and $T_{g,p}$, $T_{g,s}$ and $T_{g,m}$ are glass transition temperatures of polymer, solvent and polymer solution, respectively. Glass transition temperatures of solvents were calculated based on eqn (17).[44]

$$1.15 = \frac{T_m + T_b}{T_g + T_b} \quad (17)$$

where T_m, T_b, and T_g are melting, boiling, and glass transition temperatures.

With the view of vitrification phenomenon, our procedure of calculating the diffusion coefficients is the same as statement in Section 3.3. Only one and important difference is t_f, the time that a polymer solution needs to be completely dried. In the new approach we introduce t'_f as the time which the polymer solution transfers from rubbery to glassy state. To calculate t'_f as an unknown value, the trial and error solution method was used. Initial value for computation was inflection point of compositional curve of solvent against time, as illustrated in Fig. 13 for PS/THF system. Extending the time for calculation

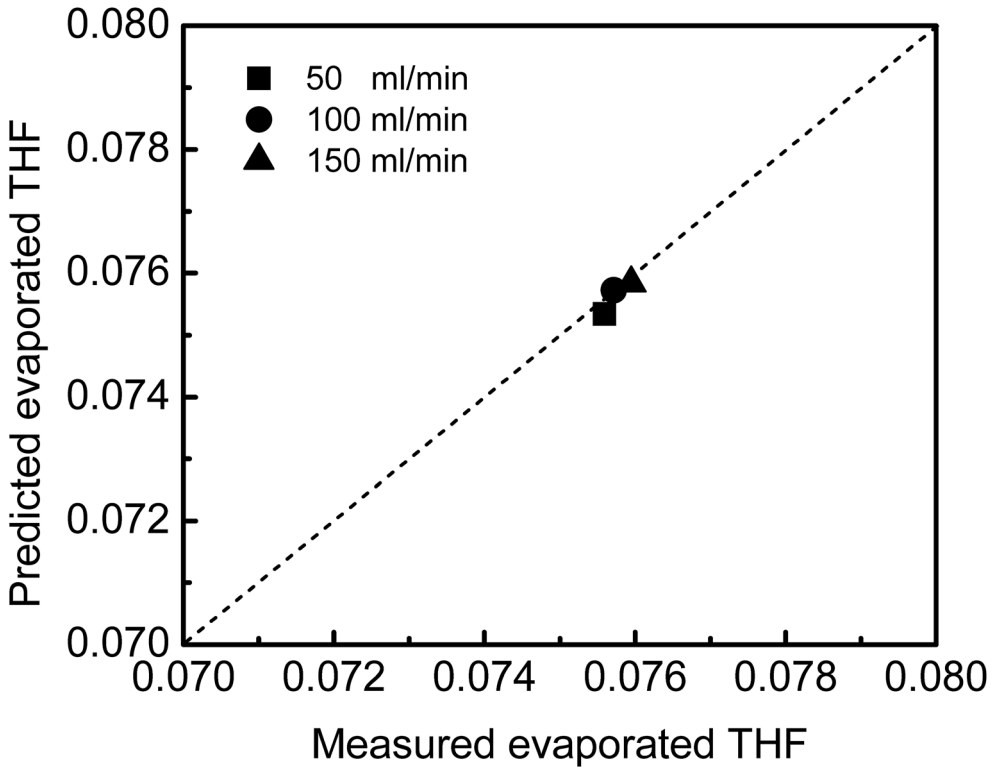

Fig. 11 Measured *versus* predicted evaporated THF from PSF with thickness of 740 μm for various flowrates at 25 °C.

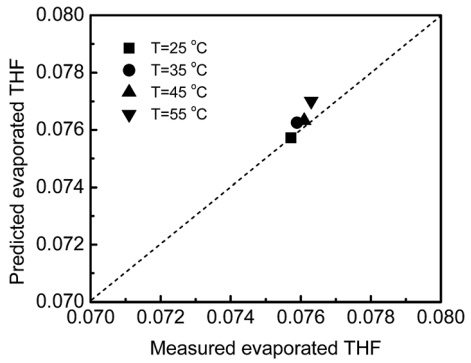

Fig. 12 Measured *versus* predicted evaporated THF from PSF with thickness of 740 μm under nitrogen flowrate of 100 ml min^{-1} and various temperatures.

Table 2 Concentration of polymer solution at $T_g = 25$ °C

Solvent	T_g (°C)	Solvent weight fraction
THF	130	0.85
$CHCl_3$	110	0.88
CH_2Cl_2	103	0.89
Toluene	116	0.88
Benzene	196	0.70
Dioxane	198	0.69
C_2Cl_4	169	0.77

was continued until significant deviation between predicted and measured concentration solvent was observed; this time is called t'_f. Then characterization of parameters in eqn (12) was carried out for seven polymer solutions in the range of $t = 0$ and $t = t'_f$, and presented in Table 3.

The comparison of both diffusion coefficients (Tables 1 and 3) follows larger values for the approach which considers the early stage of the evaporation process. Besides, a satisfying agreement is observed for the results of this approach to the literature. However the overall diffusion coefficient which is applicable in the whole range of concentration cannot exactly explain evaporation process. On the other hand, it can be concluded that the vitrification phenomenon is an important

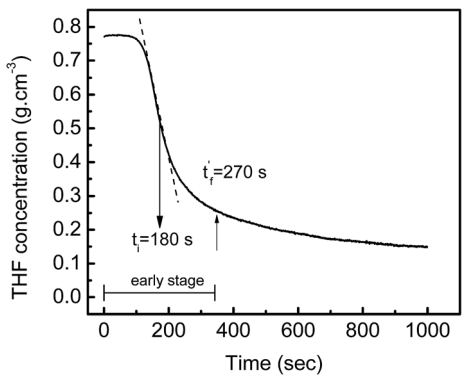

Fig. 13 Inflection point of THF concentration against time as an initial value for finding t'_f in the trial and error solution method using eqn (12).

Table 3 Diffusion coefficient of various solvents in the early stage of evaporation process

Solvent	D_0 (m^2 s^{-1})	α
THF	9.83×10^{-10}	1.9717
$CHCl_3$	1.04×10^{-09}	0.0002
CH_2Cl_2	2.40×10^{-09}	0.0006
Toluene	3.95×10^{-10}	0.5049
Benzene	1.07×10^{-09}	0.0572
Dioxane	2.28×10^{-10}	0.6877
C_2Cl_4	1.03×10^{-10}	0.8257

factor influencing the kinetics of the processes which are governed by diffusion-control.

5. Conclusions

The original purpose of this work was introduction of new approach for estimating the diffusion of small molecules like solvents in polymer/solvent mixtures. Results showed that the diffusion coefficients of seven solvents in polystyrene solutions were successfully measured using Fourier transform infrared attenuated total reflectance (FTIR-ATR) and principal component regression (PCR) analysis. A general diffusion model was adapted to experimental data of solvent evaporation. The concentrations with respect to time were applied as a boundary condition for the mass transport balance equation. The predictions for different operating conditions were generally acceptable. Diffusion coefficients of solvents were not to be as we expected; lower values for all solvents were obtained in comparison with the literature. Analyzing the early stage of mass transfer to fit the diffusion model leads to more reliable values. The reason for doing this procedure was the solidification of polymer before it becomes completely dry at the top layer of polymer solution film. Such an event is known as vitrification phenomenon. The diffusion coefficients obtained by this approach were found in good agreement with those measured by other methods.

Abbreviations and nomenclature

AC	Acetone
ATR	Attenuated total internal reflection
DCM	Dichloromethane
FTIR	Fourier transmission infrared
PCR	Principle component regression
PS	Polystyrene
PSF	Polymer solution film
TCE	Tetrachloroethylene
THF	Tetrahydrofuran
ZnSe	Zinc selenide
a	Activity fraction of solvent
C	Concentration (g cm^{-3})
C_{FTIR}	Concentration data extracted from FTIR spectra (g cm^{-3})
C_e	Concentration of solvent vapor in the air (g cm^{-3})
C_∞	Concentration of solvent vapor in ambient air (g cm^{-3})
D_0	Constant parameter of diffusion coefficient (m^2 s^{-1})
D	Diffusion coefficient (m^2 s^{-1})
D_a	Diffusion coefficient of solvent vapor in the air (m^2 s^{-1})
d_p	Penetration depth of evanescent wave (μm)
H	Height (mm)
J_s^{prd}	Flux of solvent evaporation (kg m^{-2} s^{-1})
k	Mass transfer coefficient (m s^{-1})
L	Length (mm)
m_s^{prd}	Mass of evaporated solvent (g)
n_1	Refractive index of ATR crystal
n_2	Refractive index of polymer solution
Nu	Nusselt number
OF	Objective function
Re	Reynolds number
Sc	Schmidt number
t	Time (s)
t_f	Time needed for polymer solidification (s)
T	Temperature (K)
T_g	Glass transition temperature (K)
$T_{g,mix}$	Glass transition of mixture (K)
v_p	Molar volume of polymer (cm^3 mol^{-1})
v_s	Molar volume of solvent (cm^3 mol^{-1})
w	Weight fraction
W	Width (mm)

Greek letters

α	Constant parameter
θ	Angle of incidence beam
λ	Wavelength of the infrared radiation
ρ_s	Density of solvent vapor (g cm^{-3})
φ	Volume fraction
χ	Flory–Huggins interaction parameter

Subscripts

b	Boiling temperature
FTIR	Fourier transmission infrared
m	Mixture
m	Melting temperature
p	Polymer
s	Solvent

Superscripts

prd	Predicted value

References

1 M. Karimi, *Diffusion in polymer solids and solutions*, INTECH Open Access Publisher, 2011.
2 M. Karimi and M. H. Kish, Poly(methyl methacrylate) Membrane: Dynamic Measurement of Concentrations During Water-Induced Phase Separation, in *Macromolecular symposia*, Wiley Online Library, 2009.
3 S. Azari, M. Karimi and M. Kish, Structural properties of the poly(acrylonitrile) membrane prepared with different cast thicknesses, *Ind. Eng. Chem. Res.*, 2010, **49**(5), 2442–2448.
4 H. Hajova, *et al.*, Experimental Study of Sorption and Diffusion of *n*-Pentane in Polystyrene, *J. Chem. Eng. Data*, 2013, **58**(4), 851–865.
5 A. A. Tashvigh, *et al.*, A novel approach for estimation of solvent activity in polymer solutions using genetic programming, *Calphad*, 2015, **51**, 35–41.
6 X. Liu, *et al.*, Preparation and Evaluation of a Novel pADM-derived Micro- and Nano Electrospun Collagen Membrane, *RSC Adv.*, 2015, **5**, 52079–52087.
7 L. E. Nonnekes, S. J. Cox and W. R. Rossen, Effect of Gas Diffusion on Mobility of Foam for Enhanced Oil Recovery, *Transp. Porous Media*, 2015, **106**(3), 669–689.
8 P. Van de Witte, *et al.*, Phase separation processes in polymer solutions in relation to membrane formation, *J. Membr. Sci.*, 1996, **117**(1), 1–31.
9 D. R. Lloyd, K. E. Kinzer and H. Tseng, Microporous membrane formation *via* thermally induced phase separation. I. Solid–liquid phase separation, *J. Membr. Sci.*, 1990, **52**(3), 239–261.
10 U. Ghosh, S. Kumar and S. Upadhyay, Diffusion coefficient in aqueous polymer solutions, *J. Chem. Eng. Data*, 1991, **36**(4), 413–417.
11 M. Karimi and F. Asadi, Analyzing the Diffusion Process for Polymer Solution Using FTIR-ATR Technique: Special Considerations, *Journal of Textiles and Polymers*, 2013, **1**, 1.
12 G. D. Verros, Application of non-equilibrium thermodynamics and computer aided analysis to the estimation of diffusion coefficients in polymer solutions: the solvent evaporation method, *J. Membr. Sci.*, 2009, **328**(1), 31–57.
13 G. D. Verros and G. K. Xentes, Development of a Unifying Framework for Modeling Multi-component Diffusion in Polymer Solutions, *J. Solution Chem.*, 2014, **43**(1), 206–226.
14 J. Duda, *et al.*, Prediction of diffusion coefficients for polymer-solvent systems, *AIChE J.*, 1982, **28**(2), 279–285.
15 C. Sammon and J. Yarwood, FTIR-ATR studies of the sorption and diffusion of acetone: water mixtures in poly(vinyl alcohol)–clay nanocomposites, *Polymer*, 2012, **53**(442), 0e4428.
16 C. Zeng, *et al.*, Infinite dilute activity and diffusion coefficients in polymers by inverse gas chromatography, *J. Chem. Eng. Data*, 2006, **51**(1), 93–98.
17 J. Kim and K. Lee, Prediction of mutual diffusion coefficient in polymer solution, *Polymer*, 2000, **41**(23), 8441–8448.
18 O. Karlsson, *et al.*, Estimating diffusion coefficients for small molecules in polymers and polymer solutions, *Polymer*, 2001, **42**(11), 4915–4923.
19 Q.-L. Liu and H.-Q. Gao, Prediction of mutual-diffusion coefficients in polymer solutions using a simple activity coefficient model, *J. Membr. Sci.*, 2003, **214**(1), 131–142.
20 I. S. Bayer, A. J. Davis and A. Biswas, Robust superhydrophobic surfaces from small diffusion flame treatment of hydrophobic polymers, *RSC Adv.*, 2014, **4**(1), 264–268.
21 J. G. Van Alsten and S. R. Lustig, Polymer mutual diffusion measurements using infrared ATR spectroscopy, *Macromolecules*, 1992, **25**(19), 5069–5073.
22 G. Fieldson and T. Barbari, The use of FTi. r.-atr spectroscopy to characterize penetrant diffusion in polymers, *Polymer*, 1993, **34**(6), 1146–1153.
23 Y. Fu and L.-T. Lim, Investigation of multiple-component diffusion through LLDPE film using an FTIR-ATR technique, *Polym. Test.*, 2012, **31**(1), 56–67.
24 B. D. Hanh, R. H. Neubert and S. Wartewig, Investigation of drug release from suspension using FTIR-ATR technique: part I. Determination of effective diffusion coefficient of drugs, *Int. J. Pharm.*, 2000, **204**(1), 145–150.
25 S. Hong, T. Barbari and J. Sloan, Multicomponent diffusion of methyl ethyl ketone and toluene in polyisobutylene from vapor sorption FTIR-ATR spectroscopy, *J. Polym. Sci., Part B: Polym. Phys.*, 1998, **36**(2), 337–344.
26 P. Wu and H. Siesler, Water diffusion into epoxy resin: a 2D correlation ATR-FTIR investigation, *Chem. Phys. Lett.*, 2003, **374**(1), 74–78.
27 C. Wang, *et al.*, Research on Mechanical Properties of Different Fibers Reinforced Biomass Composites Based on Chemical Bonds, *RSC Adv.*, 2015, **5**, 49824–49830.
28 Y. A. Elabd, M. G. Baschetti and T. A. Barbari, Time-resolved Fourier transform infrared/attenuated total reflection spectroscopy for the measurement of molecular diffusion in polymers, *J. Polym. Sci., Part B: Polym. Phys.*, 2003, **41**(22), 2794–2807.
29 M. W. Urban, *Attenuated total reflectance spectroscopy of polymers: theory and practice*, American Chemical Society, 1996.
30 N. J. Harrick, *Internal reflection spectroscopy*, Harrick Scientific Corp, 1967.
31 I. Jolliffe, *Principal component analysis*, Wiley Online Library, 2005.
32 R. B. Bird, W. E. Stewart and E. N. Lightfoot, *Transport phenomena*, John Wiley & Sons, 2007.
33 R. E. Treybal and E. Treybal Robert, *Mass-transfer operations*, McGraw-Hill, New York, 1968, vol. 3.
34 P. J. Flory, Thermodynamics of high polymer solutions, *J. Chem. Phys.*, 1942, **10**(1), 51–61.
35 B. Cao and M. A. Henson, Modeling of spiral wound pervaporation modules with application to the separation of styrene/ethylbenzene mixtures, *J. Membr. Sci.*, 2002, **197**(1), 117–146.

36 F. Lipnizki and G. Trägårdh, Modelling of pervaporation: models to analyze and predict the mass transport in pervaporation, *Sep. Purif. Rev.*, 2001, **30**(1), 49–125.
37 K. W. Böddeker, *Pervaporation durch Membranen und ihre Anwendung zur Trennung von Flüssiggemischen*, VDI-Verlag, 1986.
38 F. Greenlaw, R. Shelden and E. Thompson, Dependence of diffusive permeation rates on upstream and downstream pressures: II. Two component permeant, *J. Membr. Sci.*, 1977, **2**, 333–348.
39 F. Greenlaw, *et al.*, Dependence of diffusive permeation rates on upstream and downstream pressures: I. Single component permeant, *J. Membr. Sci.*, 1977, **2**, 141–151.
40 R. Y. Huang and V. J. Lin, Separation of liquid mixtures by using polymer membranes. I. Permeation of binary organic liquid mixtures through polyethylene, *J. Appl. Polym. Sci.*, 1968, **12**(12), 2615–2631.
41 R. A. Sferrazza, R. Escobosa and C. H. Gooding, Estimation of parameters in a sorption-diffusion model of pervaporation, *J. Membr. Sci.*, 1988, **35**, 125–136.
42 D. J. Higham and N. J. Higham, *MATLAB guide*, Siam, 2005.
43 A. Asadi Tashvigh, F. Zokaee Ashtiani and A. Fouladitajar, Genetic programming for modeling and optimization of gas sparging assisted microfiltration of oil-in-water emulsion, *Desalin. Water Treat.*, 2015, 1–11.
44 M. Mulder, *Basic Principles of Membrane Technology*, Kluwer Academic Pub, 2nd edn, 1996.